

Visualizing extended defects at the atomic level in a $Bi_2Sr_2CaCu_2O_{8+\delta}$ superconducting wire

Kejun Hu(胡柯钧), Shuai Wang(王帅), Boyu Li(李泊玉), Ying Liu(刘影), Binghui Ge(葛炳辉), and Dongsheng Song(宋东升)

Citation: Chin. Phys. B, 2024, 33 (**9**): 096101. DOI: 10.1088/1674-1056/ad6ccd
Journal homepage: http://cpb.iphy.ac.cn; http://iopscience.iop.org/cpb

What follows is a list of articles you may be interested in

Electronic effects on radiation damage in α-iron: A molecular dynamics study

Lin Jiang(江林), Min Li(李敏), Bao-Qin Fu(付宝勤), Jie-Chao Cui(崔节超), and Qing Hou(侯氢)
Chin. Phys. B, 2024, 33 (**3**): 036103. DOI: 10.1088/1674-1056/ad0ec4

Geometries and electronic structures of $Zr_nCu(n$ =2-12) clusters: A joint machine-learning potential density functional theory investigation

Yizhi Wang(王一志), Xiuhua Cui(崔秀花), Jing Liu(刘静), Qun Jing(井群), Haiming Duan(段海明), and Haibin Cao(曹海宾)
Chin. Phys. B, 2024, 33 (**1**): 016109. DOI: 10.1088/1674-1056/acd5c2

Analysis of displacement damage effects on the charge-coupled device induced by neutrons at Back-n in the China Spallation Neutron Source

Yuan-Yuan Xue(薛院院), Zu-Jun Wang(王祖军), Wei Chen(陈伟), Xiao-Qiang Guo(郭晓强), Zhi-Bin Yao(姚志斌), Bao-Ping He(何宝平), Xu Nie(聂栩), Shankun Lai(赖善坤), Gang Huang(黄港), Jiang-Kun Sheng(盛江坤), Wu-Ying Ma(马武英), and Shi-Long Gou(缑石龙)
Chin. Phys. B, 2023, 32 (**7**): 076101. DOI: 10.1088/1674-1056/acac07

Dislocation mechanism of $Ni_{47}Co_{53}$ alloy during rapid solidification

Yun-Chun Liu(刘云春), Yong-Chao Liang(梁永超), Qian Chen(陈茜), Li Zhang(张利), Jia-Jun Ma(马家君), Bei Wang(王蓓), Ting-Hong Gao(高廷红), and Quan Xie(谢泉)
Chin. Phys. B, 2023, 32 (**6**): 066104. DOI: 10.1088/1674-1056/aca7ea

Low temperature *Pmmm* and *C*2/*m* phases in $Sr_2CuO_{3+\delta}$ high temperature superconductor

Hai-Bo Wang(王海波), Zhen-Lin Luo(罗震林), Yuan-Jun Yang(杨远俊), Qing-Qing Liu(刘清青), Si-Xia Hu(胡思侠), Meng-Meng Yang(杨蒙蒙), Chang-Qing Jin(靳常青), Chen Gao(高琛)
Chin. Phys. B, 2019, 28 (**5**): 056103. DOI: 10.1088/1674-1056/28/5/056103

SPECIAL TOPIC — Stephen J. Pennycook: A research life in atomic-resolution STEM and EELS

Visualizing extended defects at the atomic level in a $Bi_2Sr_2CaCu_2O_{8+\delta}$ superconducting wire

Kejun Hu(胡柯钧), Shuai Wang(王帅), Boyu Li(李泊玉), Ying Liu(刘影)[†], Binghui Ge(葛炳辉), and Dongsheng Song(宋东升)[‡]

Information Materials and Intelligent Sensing Laboratory of Anhui Province, Key Laboratory of Structure and Functional Regulation of Hybrid Materials of Ministry of Education, Institutes of Physical Science and Information Technology, Anhui University, Hefei 230601, *China*

(Received 3 June 2024; revised manuscript received 6 August 2024; accepted manuscript online 8 August 2024)

The microstructure significantly influences the superconducting properties. Herein, the defect structures and atomic arrangements in high-temperature $Bi_2Sr_2CaCu_2O_{8+\delta}$ (Bi-2212) superconducting wire are directly characterized via state-of-the-art scanning transmission electron microscopy. Interstitial oxygen atoms are observed in both the charge reservoir layers and grain boundaries in the doped superconductor. Inclusion phases with varied numbers of CuO_2 layers are found, and twist interfaces with different angles are identified. This study provides insights into the structures of Bi-2212 wire and lays the groundwork for guiding the design of microstructures and optimizing the production methods to enhance superconducting performance.

Keywords: superconductor, microstructure, defect, scanning transmission electron microscopy

PACS: 61.05.–a, 61.72.–y, 74.62.Dh, 84.71.Mn **DOI:** 10.1088/1674-1056/ad6ccd

1. Introduction

High-temperature superconductor $Bi_2Sr_2CaCu_2O_{8+\delta}$ (Bi-2212) is known for its high critical temperature (T_c) of about 85 K–95 K, high critical currents, and high irreversibility field.[1–5] These characteristics position Bi-2212 as a leading first-generation commercial superconducting material, making it a promising candidate for applications in magnetic resonance imaging (MRI), particle accelerators, and high-energy physics magnets, where high critical current density and high critical magnetic field are crucial.[6–8]

However, as ceramic compounds, these high-temperature superconducting oxides are inherently fragile in texture. To enhance their mechanical properties and broaden the application of Bi-based superconducting materials, various preparation methods have been explored.[9–12] Currently, the preparation of Bi-2212 superconducting wire typically employs the powder-in-tube (PIT) method with an Ag sheath.[12,13] During the melting heat treatment, the Bi-2212 precursor powder, initially of low connectivity, transforms into a well-connected Bi-2212 grain network, resulting in higher density and improved textural grains.[14] The Ag sheath allows oxygen to permeate during the high-temperature heat treatment, thereby regulating the oxygen content in the superconductor. The interstitial oxygen doping is influenced by the modulation structure and changes in the CuO_2 plane structure, which is crucial for developing superconducting properties.[15–19] Given the complex phase structure and significant oxygen doping in Bi-2212, a detailed examination of its microstructure and defects is essential, as these factors directly influence its superconducting properties.[20–22] Moreover, the analysis of the microstructure and defects in Bi-2212 superconducting wires is vital for enhancing their performance and reliability through tailored synthesis and processing techniques.

In this paper, the state-of-the-art scanning transmission electron microscopy (STEM) and integrated differential phase contrast (iDPC) techniques are employed to directly image the defect structure and atomic arrangements in a commercial Bi-2212 superconducting wire. The doped oxygen atoms are found both in the charge reservoir layers and at the grain boundaries. Dislocations are observed to penetrate the superconducting layers and the stacking defects with specific twist angles are identified in the wire.

2. Methods

The cross-sectional TEM lamellas of $Bi_2Sr_2CaCu_2O_{8+\delta}$ were thinned to electron beam transparency at 30 kV by using Carl Zeiss Crossbeam 550L FIB-SEM, followed by the removal of the surface amorphous layer at 2 kV. The high-angle annular dark field STEM (HAADF-STEM) and iDPC-STEM experiments were conducted using a Thermo Fischer Scientific Titan Themis Z microscope operating at 300 kV, equipped with a probe corrector and a four-segment DF4 detector. The convergence semi-angle for imaging is 25 mrad, and the collection semi-angle is 50 mrad–200 mrad for HAADF imaging and 8 mrad–42 mrad for iDPC. Transmission Kikuchi diffraction (TKD) experiments were performed on TEM specimens

[†]Corresponding author. E-mail: liuying.hube@outlook.com
[‡]Corresponding author. E-mail: dsong@ahu.edu.cn

© 2024 Chinese Physical Society and IOP Publishing Ltd

within the FIB-SEM.

3. Results and discussion

In Bi-2212 superconducting wire, the superconducting core is composed of numerous well-oriented Bi-2212 filaments.[23] Each filament contains the Bi-2212 phase after heat treatment. Weak connections, such as large-angle grain boundaries, can be minimized or eliminated in these filaments by preferentially aligning the grains along the *ab* plane to form a textured structure.[24] This alignment increases the material's density, and enhances the grain connectivity, as shown in the low-magnification STEM image in Fig. 1(a). The texture configuration is crucial for the smooth passage of the superconducting current through the grain boundaries. Therefore, reducing the current loss at these boundaries is essential to increase the critical current density. In Fig. 1(b), the TKD analysis reveals that these textured grains are stacked along the *c*-axis direction, with significant twists in the *ab* plane, as indicated by the interface between the red and orange regions in the orientation map (OM). Small-angle grain boundaries are also present in the filament, as indicated by the interface between the orange and pink regions.

Bi-2212 exhibits a two-dimensional layered structure with alternating charge reservoir layers and superconducting CuO_2 layers. The charge reservoir layer consists of stacked SrO–BiO–BiO–SrO planes, while the superconducting layer comprises two CuO_2 planes separated by Ca layers, as depicted in the atomic models (excluding oxygen atoms) in Figs. 1(c) and 1(d) along the [100] and [010] directions, respectively. Incommensurate modulation structure is clearly observed along the [010] direction, which is believed to originate from the misfit between the perovskite planes (CuO_2 and SrO) and the rock-salt planes (BiO) in the crystal.[25–27] The corresponding HAADF-STEM images are displayed in Figs. 1(e) and 1(f) with only the heavy elements visible. Significant lattice distortion and incommensurate modulation structure are observed in Fig. 1(f) with substantial atomic fluctuations. The BiO layers exhibit tensile and compressive strain states at the necking and bumped regions, respectively.[28]

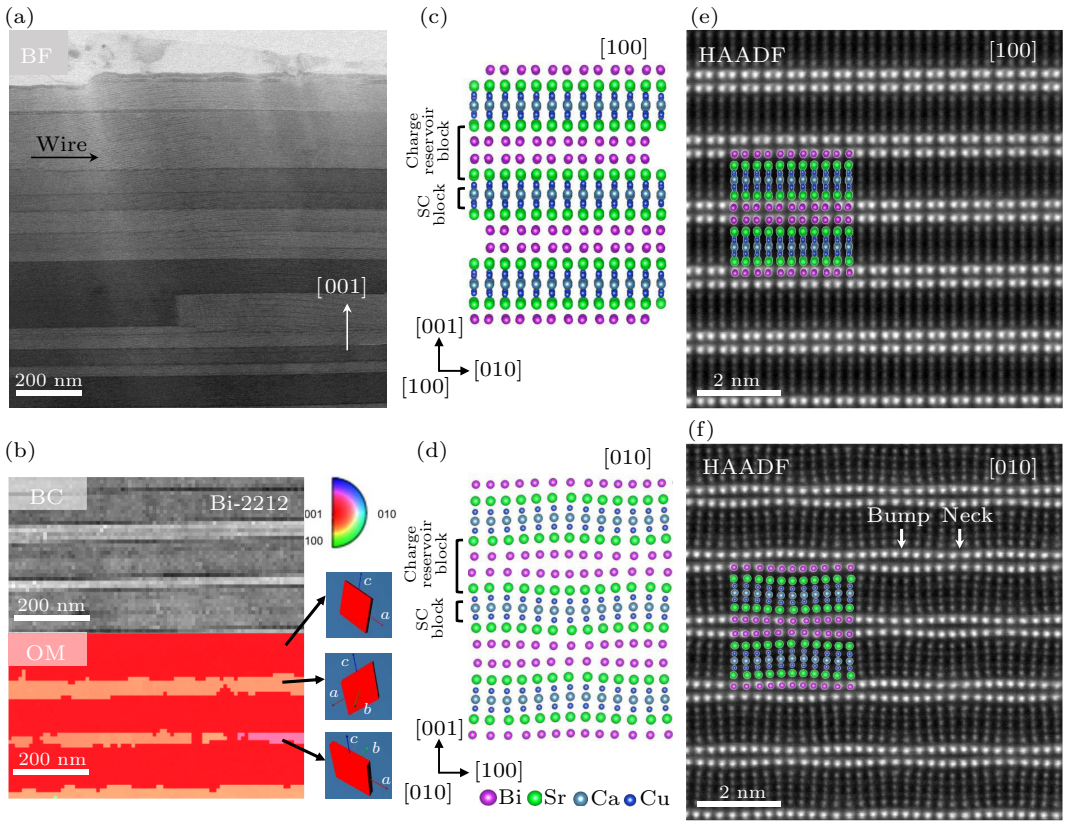


Fig. 1. (a) BF-STEM image of the cross-section of the Bi-2212 wire texture structure at low magnification. (b) TKD analysis of Bi-2212, including band contrast (BC) and orientation map (OM). (c) Atomic structure model along [100] (oxygen atoms not shown). (d) Atomic structure model along [010] (oxygen atoms not shown). (e) HAADF-STEM image of Bi-2212 along [100] orientation. (f) HAADF-STEM image of Bi-2212 along [010] orientation.

For Bi-based superconductors, the critical transition temperature (T_c) can be influenced by both the concentration of hole carriers in the CuO_2 plane and the number of CuO_2 layers (n) in a unit cell.[29,30] Generally, an increase in the number of CuO_2 layers leads to a higher T_c: $n = 1$ ($\sim$ 10 K),[31] $n = 2$ ($\sim$ 85 K),[3] $n = 3$ ($\sim$ 110 K).[1] However, when $n > 3$, such as in Bi-2234, the material becomes more challenging to synthesize, and T_c decreases.[32] Additionally, for a fixed

number of CuO_2 layers, the highest T_c is achieved at optimal oxygen doping. Therefore, it is essential for us to examine the CuO_2 layers and the doped oxygen atoms in the superconducting wires. As shown in Figs. 2(a) and 2(c), only a small amount of Bi-2201 is found as an inclusion in Bi-2212 phase, fully coherent along the *c*-axis direction. Despite the presence of Bi-2201 phase, the pronounced modulation structure is still well kept. After examining the entire sample, no other phases with varying numbers of CuO_2 layers were observed, indicating the high purity of the Bi-2212 phase. During the preparation process, it is believed that the Bi-2201 phase is formed as a result of the instability of Bi-2212 at the partial melting heat treatment temperature.

Due to the distortion induced by this modulated structure, the spacing between atomic layers undergoes significant changes, creating favorable sites for interstitial oxygen atoms. Previous studies have reported that doped oxygen atoms are energetically favored at the necking regions between the two BiO layers.[28] The presence of these excess oxygen atoms can significantly affect the hole concentration in the material, thus influencing superconductivity. Therefore, we utilized the advanced iDPC-STEM technique, with the capability of imaging light and heavy elements simultaneously,[33] to characterize interstitial oxygen atoms in Bi-2212 and Bi-2201, as depicted in Figs. 2(b) and 2(d). Except for the oxygen atoms in the CuO_2 layers, interstitial oxygen atoms with weak contrast were observed in both Bi-2201 and Bi-2212, exhibiting a random distribution at the necking regions. These findings indicate that oxygen atoms were successfully doped into the charge reservoir layers during the post-heat treatment. Although the amount of doped oxygen atoms cannot be quantified by STEM at present, optimal doping can be achieved by optimizing the T_c during the process.

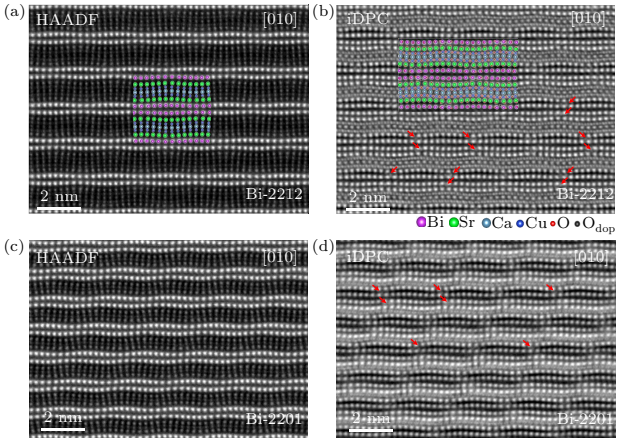


Fig. 2. (a) HAADF-STEM image of Bi-2212 along [010] orientation. (b) iDPC-STEM image corresponding to panel (a), where the red arrows represent the doped interstitial oxygen atoms. (c) HAADF-STEM image of Bi-2201 along [010] orientation. (d) The iDPC-STEM image corresponding to panel (c), where the red arrows represent the doped interstitial oxygen atoms.

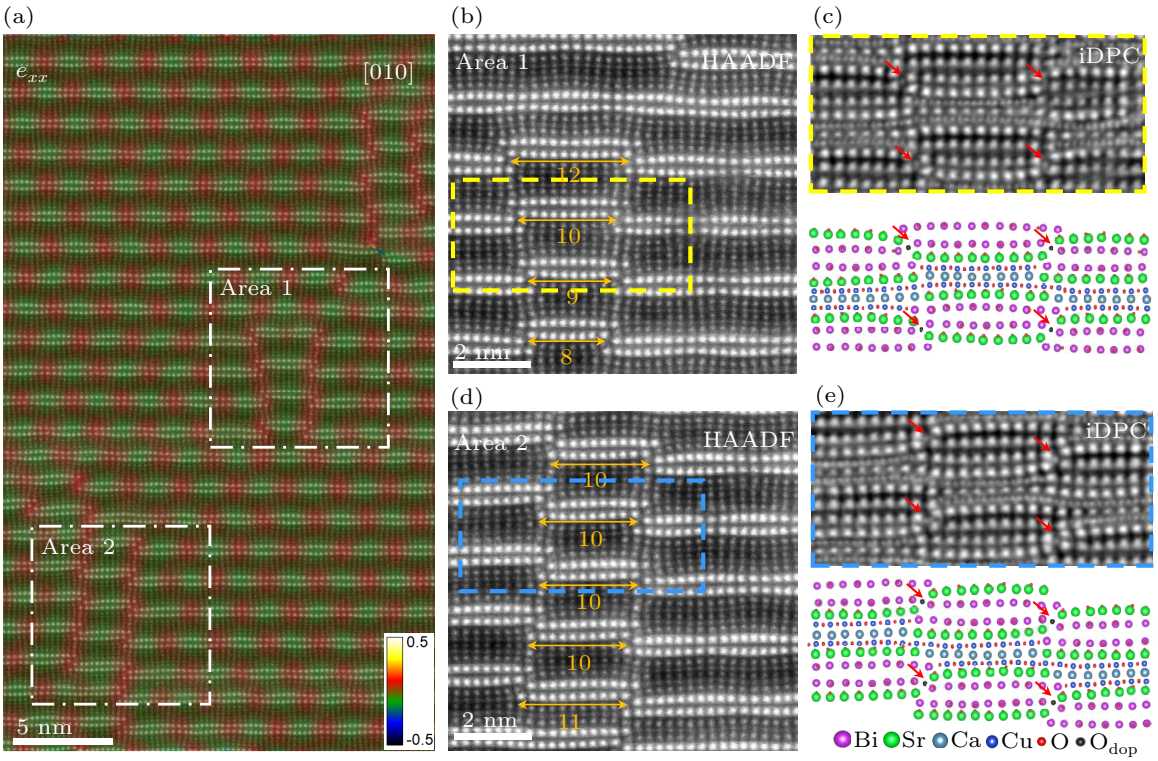


Fig. 3. (a) HAADF-STEM image of Bi-2212 with misaligned atomic planes in the [010] orientation, with the strain e_{xx} calculated by GPA[35] superimposed on the HAADF image. (b) Enlarged HAADF image of area 1 in panel (a), with orange arrows indicating the number of misaligned atomic columns. (c) iDPC image corresponding to the yellow dotted box in panel (b), with the atomic structure model of the corresponding region below. (d) Enlarged HAADF image of area 2 in panel (a), with orange arrows indicating the number of misaligned atomic columns. (e) iDPC image corresponding to the blue dashed box in panel (d), with the atomic structure model of the corresponding region below.

Although large-angle grain boundaries have been largely eliminated during the heat treatment, a large number of faults in atomic planes along the [001] direction are found in Bi-2212, introducing new boundaries as indicated by the white dashed box in Fig. 3(a). The presence of these faults is attributed to the different numbers of CuO_2 layers between Bi-2201 and Bi-2212. The width of these boundaries is evaluated by counting the number of Bi atoms along the [100] direction. Two typical regions with varied widths are enlarged in Figs. 3(b) and 3(d). In area 1 of Fig. 3(b), the modulation period of the disordered atomic plane gradually decreases from top to bottom, displaying a "reverse ladder type" pattern. In area 2 of Fig. 3(d), the modulation period of the disordered atomic plane remains nearly constant from top to bottom. Interestingly, these boundaries always occur close to the necking regions of the BiO layers, likely owing to the tensile strain states that accommodate the local mismatch. Given that the necking region of Bi-2212 is energetically favorable for doped oxygen atoms, we employed the iDPC-STEM technique to identify interstitial oxygen, as indicated by the red arrows in Figs. 3(c) and 3(e). The oxygen contrast appears at almost all of these sites, in contrast to the random distribution in pure Bi-2212 phases. These findings suggest that defective boundaries do not diminish the concentration of charge carriers. The facile doping of oxygen atoms at these boundaries can be attributed to locally high tensible strain states, which energetically favor accommodating oxygen dopants. The proper concentration of doped oxygen atoms is crucial for cuprate superconductors. Moreover, unlike typical large- or small-angle grain boundaries in polycrystalline samples, which invariably act as weak links in superconductivity, the layered structure remains largely intact across these boundaries here, thereby minimizing their impact on superconductivity. This resilience is particularly important to cuprate superconductors with a relatively short coherence length.

However, the CuO_2 planes can either run through the boundaries in area 1 or be disrupted by the boundaries in area 2, depending on the shift of atomic planes along the [001] directions. Compared to the pure Bi-2212 phase, the number of CuO_2 layers is reduced, and the flatness of these layers is strongly distorted, as shown in the atomic model in Figs. 3(c) and 3(e). This distortion might suppress superconductivity as it will decrease the antiferromagnetic super-exchange interaction, which is believed to play the role of cooper pairing glue in the framework of local superconducting theory.[34] Therefore, these defects should be eliminated as much as possible during synthesis.

Due to its layered configuration, Bi-2212 is susceptible to stacking defects during growth, leading to the formation of twisted interfaces. These twisted interfaces offer a platform for engineering superconducting ordering parameters by adjusting the stacking angles. Previous studies have demonstrated Josephson coupling in Bi-2212 superconductor with a twist angle of 45° (in plane rotation from [010] to [110]).[36] In Bi-2212 superconducting wire, the layered structure with varied twist angles is observed, as shown in Fig. 4. In Fig. 4(a), an interface with a twist angle of 90° is formed between the [100] and [010] oriented grains. This interface is atomically sharp, and the first BiO layer in the [100] oriented grain is strongly distorted to match the modulation in the [010] oriented grain, enabling an abrupt transition. In addition, interfaces with varied twist angles are observed in Figs. 4(b) and 4(c). The orientation of the bottom grain deviates from the low-index zone axis while still displaying the incommensurate modulation structure. Moreover, despite these coherent interfaces stacked along the [001] direction, grain boundaries in the *ab* plane are also observed in Fig. 4(d) due to the misalignment in the [001] direction. These grain boundaries could significantly suppress superconductivity due to the atomic disorders and interruption of CuO_2 planes.

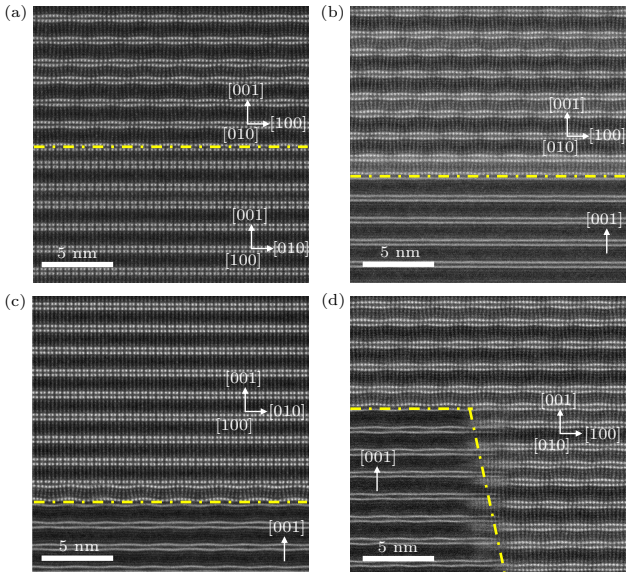


Fig. 4. (a) Grains with [010] orientation (top) and [100] orientation (bottom) form a twist angle of 90° at the interface. (b) Twist angle formed between grains oriented [010] and grains with high-index axes. (c) Twist angle formed between grains oriented [100] and grains with high-index axes. (d) Twist angle formed by [010] oriented grains with high-index axes and small-angle grain boundaries.

Based on these experimental observations, these defects can be categorized into two main types: the stacking faults along the *c* axis throughout the samples and vertical misalignment at the boundaries, with rough estimated line density of $\sim 1.6 \times 10^5$ per cm and area density of $\sim 1.0 \times 10^8$ per cm^2, respectively. While these defects might suppress local superconductivity due to the altered flatness of CuO_2 planes and the charge carrier density, they might also serve as effective pinning centers for magnetic flux flow, thereby enhancing the critical current density and irreversibility field.[37] Understand-

ing the interaction between these atomic-scale and microstructural defects and magnetic vortices would facilitate the design of materials performance for achieving exceptional superconducting properties in practical application.

4. Conclusion

In summary, we utilized advanced scanning transmission electron microscopy to characterize the atomic structure of Bi-2212 superconducting wire through HAADF-STEM and iDPC-STEM imaging techniques. Our findings revealed the rich defect structures in the wire, including the doped oxygen atoms, Bi-2201 inclusion, phase boundaries, and twist interfaces. This detailed microstructural understanding provides a foundation for advancing the high-temperature superconductor technology, guiding the design of new materials, and optimizing production methods to meet the demands of high-field applications.

References

[1] Maeda H, Tanaka Y, Fukutomi M and Asano T 1988 *Jpn. J. Appl. Phys.* **27** L209

[2] Gao Y, Lee P, Coppens P, Subramania M A and Sleight A W 1988 *Science* **241** 954

[3] Sunshine S A, Siegrist T, Schneemeyer L F, Murphy D W, Cava R J, Batlogg B, van Dover R B, Fleming R M, Glarum S H, Nakahara S, Farrow R, Krajewski J J, Zahurak S M, Waszczak J V, Marshall J H, Marsh P, Rupp L W and Peck W F 1988 *Phys. Rev. B* **38** 893

[4] Zhao J, Gan Y L, Yang G, Zhong Y G, Tang C Y, Yang F Z, Phan G N, Sui Q T, Liu Z, Li G, Qiu X G, Zhang Q H, Shen J, Qian T, Lu L, Yan L, Gu G D and Ding H 2022 *Chin. Phys. Lett.* **39** 077403

[5] Liu W, Zha H, Gu G D, Shen X, Ye M and Qiao S 2023 *Chin. Phys. Lett.* **40** 037402

[6] Hull J R, Wilson M N, Bottura L, Rossi L, Green M A, Iwasa Y, Hahn S, Duchateau J L and Kalsi S S 2015 *Applied Superconductivity: Handbook on Devices and Applications* pp. 403–602

[7] Luo X, Chen H, Li Y, Gao Q, Yin C, Yan H, Miao T, Luo H, Shu Y, Chen Y, Lin C, Zhang S, Wang Z, Zhang F, Yang F, Peng Q, Liu G, Zhao L, Xu Z, Xiang T and Zhou X J 2023 *Nat. Phys.* **19** 1841

[8] Markiewicz W D, Miller J R, Schwartz J, Trociewitz U P and Weijers H W 2006 *IEEE Transactions on Applied Superconductivity* **16** 1523

[9] David A C and David S G 2002 *Handbook of Superconducting Materials* (1st Ed.)

[10] Hasegawa T, Koizumi T, Aoki Y, Kitaguchi H, Miao H, Kumakura H and Togano K 1999 *IEEE Transactions on Applied Superconductivity* **9** 1884

[11] Okada M, Tanaka K, Wakuda T, Ohata K, Sato J, Kumakura H, Kiyoshi T, Kitaguchi H, Togano K and Wada H 1999 *IEEE Transactions on Applied Superconductivity* **9** 1904

[12] Shen T, Jiang J, Kametani F, Trociewitz U P, Larbalestier D C, Schwartz J and Hellstrom E E 2010 *Supercon. Sci. Technol.* **23** 025009

[13] Feng Y and Larbalestier D C 1994 *Interface Sci.* **1** 401

[14] Li P, Naderi G, Schwartz J and Shen T 2017 *Supercon. Sci. Technol.* **30** 035004

[15] Presland M R, Tallon J L, Buckley R G, Liu R S and Flower N E 1991 *Physica C* **176** 95

[16] Slezak J A, Lee J, Wang M, McElroy K, Fujita K, Andersen B M, Hirschfeld P J, Eisaki H, Uchida S and Davis J C 2008 *Proc. Natl. Acad. Sci. USA* **105** 3203

[17] Johnston S, Vernay F and Devereaux T P 2009 *Europhys. Lett.* **86** 37007

[18] Khaliullin G, Mori M, Tohyama T and Maekawa S 2010 *Phys. Rev. Lett.* **105** 257005

[19] He Y, Nunner T, Hirschfeld P and Cheng H P 2006 *Phys. Rev. Lett.* **96** 197002

[20] Yan H, Gao Q, Song C, Yin C, Chen Y, Zhang F, Yang F, Zhang S, Peng Q, Liu G, Zhao L, Xu Z and Zhou X J 2022 *Chin. Phys. B* **31** 087401

[21] Yu Y, Ma L, Cai P, Zhong R, Ye C, Shen J, Gu G D, Chen X H and Zhang Y 2019 *Nature* **575** 156

[22] Massee F, Huang Y K and Aprili M 2020 *Science* **367** 68

[23] Maeda H 1996 *Bismuth-Based High-Temperature Superconductors*

[24] Jin S, Tiefel T H, Sherwood R C, Davis M E, van Dover R B, Kammlott G W, Fastnacht R A and Keith H D 1988 *Appl. Phys. Lett.* **52** 2074

[25] Fan W and Zeng Z 2011 *Supercon. Sci. Technol.* **24** 105007

[26] He Y, Graser S, Hirschfeld P J and Cheng H P 2008 *Phys. Rev. B* **77** 220507

[27] Zhiqiang M, Gaojie X, Shuyuan Z, Shun T, Bin L, Mingliang T, Chenggao F, Cunyi X and Yuheng Z 1997 *Phys. Rev. B* **55** 9130

[28] Song D, Zhang X, Lian C, Liu H, Alexandrou I, Lazić I, Bosch E G T, Zhang D, Wang L, Yu R, Cheng Z, Song C, Ma X, Duan W, Xue Q and Zhu J 2019 *Advanced Functional Materials* **29** 1903843

[29] Wang Z, Zou C, Lin C, Luo X, Yan H, Yin C, Xu Y, Zhou X, Wang Y and Zhu J 2023 *Science* **381** 227

[30] Keimer B, Kivelson S A, Norman M R, Uchida S and Zaanen J 2015 *Nature* **518** 179

[31] Maeda A, Hase M, Tsukada I I, Noda K, Takebayashi S and Uchinokura K 1990 *Phys. Rev. B* **41** 6418

[32] Chakravarty S, Kee H Y and Völker K 2004 *Nature* **428** 53

[33] Yücelen E, Lazić I and Bosch E G T 2018 *Sci. Rep.* **8** 2676

[34] Lin R, Wang Q, Song D, He C, Hu K, Liang Z, Du H, Hao N, Ge B and Wen H H 2023 *Adv. Mater.* **35** 2301021

[35] Htch M J, Snoeck E and Kilaas R 1998 *Ultramicroscopy* **74** 131

[36] Zhao S Y F, Cui X, Volkov P A, Yoo H, Lee S, Gardener J A, Akey A J, Engelke R, Ronen Y, Zhong R, Gu G, Plugge S, Tummuru T, Kim M, Franz M, Pixley J H, Poccia N and Kim P 2023 *Science* **382** 1422

[37] Teresa P, Gutierrez J and Obradors X 2023 *Nat. Rev. Phys.* **6** 132